

TEM in Geology. Basics and applications

Fernando Nieto García

Departamento de Mineralogía y Petrología and IACT, Universidad de Granada-CSIC,
18002 Granada, Spain

Introduction

In general a microscope is capable of producing an enlarged image of an object through a combination of lenses. The fundamental lens is the objective lens, which produces a diffraction pattern of the object in its back-focal plane. If these diffracted beams are focused and magnified again by additional lenses, we finally obtain the enlarged image of the object. This is the normal means of operation of an optical microscope (Fig. 1). The resolution of the microscope depends on the wavelength of the radiation used. Therefore, the resolution of an optical microscope is limited to textural relationships between crystalline objects, but it is unable to provide information about the atomic structure of these crystalline objects. In theory, X-rays and electrons have wavelengths small enough to produce such information. Consequently, these two types of radiation are usually employed to study the crystalline structure of matter. Nevertheless, no lenses exist for X-rays; therefore, they cannot be focused to produce an image and X-rays microscopes do not exist. An X-ray “image” can only be generated by crystallographers by calculating the intensity of the diffracted beams; however, in the electron microscope, the Fourier transform of the diffracted beams is physically carried out by the electromagnetic lenses and a real image can be obtained. The geometry and optical paths of the rays in optical and electron microscopes are exactly equivalent (Fig. 1).

A significant difference between these two types of microscopes is that electromagnetic lenses can continuously change their focal length, and thus their magnification, in contrast to glass lenses. Some consequences are easily deduced, but perhaps the fundamental one is the possibility of bringing to the image plane the back focal plane of the objective lens—that is, the diffraction pattern instead of the

intermediate image (Fig. 1). In modern microscopes, the change from image to diffraction can be accomplished instantly by pressing a button.

When electrons interact with matter, other signals (in addition to various types of electrons) such as electromagnetic waves are produced. Analytically, X-rays are the most important, as their wavelength contains the fingerprint of the chemical elements present in the sample. This is the basis of all the modern *in-situ* analytical techniques. Although electron microprobe and scanning electron microscopes with EDX are the best-known examples of such techniques, this possibility is also present in the transmission electron microscope (TEM).

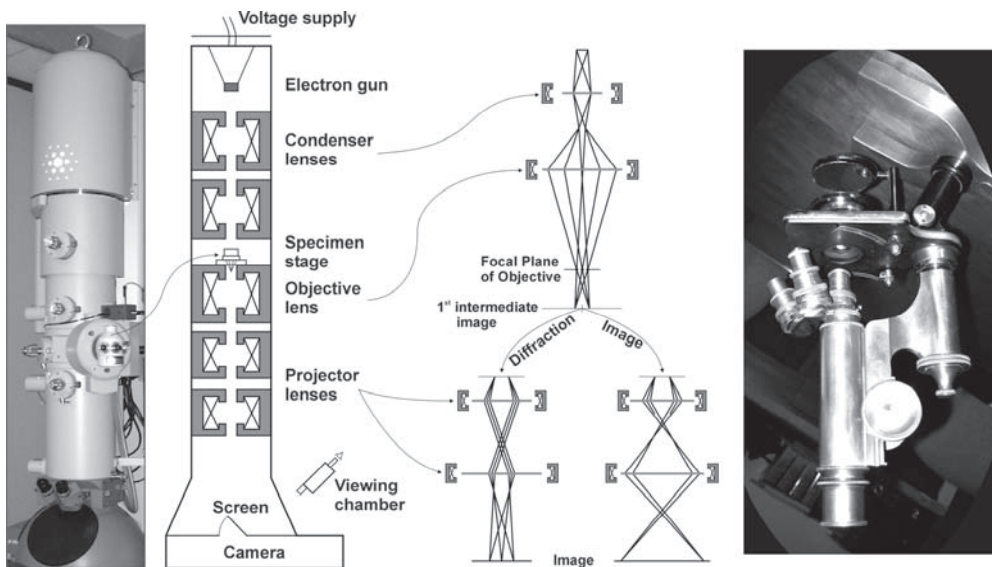


FIGURE 1. Schematic of the column of a transmission electron microscope (left) and optical path of the rays valid for both electron and optical microscopes (right). Two different field strengths of the projector lenses allow the production of two different ray paths after the first intermediate image. Thus, it is possible to bring to the image plane the back focal plane of the objective lens (diffraction pattern) or the intermediate image to obtain diffraction or an image, respectively. Modified from Buseck (1992) and Putnis (1993).

In conclusion, a TEM is a complex machine that simultaneously combines a powerful microscope with crystalline-lattice resolution, a diffractometer, and a chemical-analysis device. More than its high spatial resolution, this combination of techniques is the real reason for its powerful capability for geological research.

Samples

Although a universal electron microscope is possible, transmission and scanning/microprobe capabilities are, in practice, separate techniques. One of the reasons is the different characteristics of the samples involved. TEM samples must be as thin as possible. Three means of preparation are the most common for geological samples:

1) Ion milling. This technique allows the extraction of a small area from a thin section, prepared with adhesive easily melted by heat. A copper ring is affixed to the selected area with the aid of a microscope, the rock is cut around the ring, and the round piece of sample removed from the thin section by heating. The copper ring with the attached piece of rock is placed into the ion mill, which bombards the centre of the ring with a beam of ions or uncharged atoms (Fig. 2). The area surrounding the hole produced in the centre of the sample contains sectors thin enough to be studied by TEM.

2) Fine powder deposited on a holey-carbon film. This is the simplest method, very useful when neither a particular orientation of the sample nor especially thin areas are necessary. The disadvantage for petrographic studies is that information on the location of the studied grain in the rock is lost. It is a very useful method for chemical analysis of fine-grained materials.

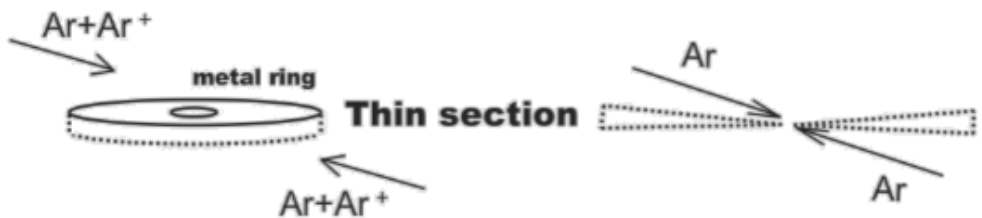


FIGURE 2. Basics of ion-milling preparation of samples. A round piece of rock, removed from the thin section by heating, is placed in the ion mill, which bombards the centre of the ring with a beam of ions or uncharged atoms (left). Sectors thin enough to be studied by TEM surround the hole thus produced (right).

3) Ultramicrotomy. This is a method widely used in bio-medical sciences. Suitable minerals either have to be relatively soft, like many layer silicates, or very fine-grained. The sample can be encased within a suitable epoxy and then sliced, like ham in a delicatessen, producing extremely thin wafers, which are deposited in a grid.

Electron diffraction

The Ewald sphere, which allows prediction of the directions of the diffracted beams, is far larger for electrons than for X-rays as a consequence of the difference in wavelength between the two kinds of radiations (Fig. 3a). Therefore, the radius of the sphere with TEM is so large and the crystal so thin (causing the diffraction spots to become spikes) that the pattern is essentially tangent over a large region of the reciprocal space and many diffraction spots can be recorded without any sample motion. In combination with the strong diffraction effects that occur with electrons, this means that planes through reciprocal space can be viewed in real time. In contrast to X-ray diffraction, diffracted electrons have a greater probability of themselves being scattered as they pass through the sample. Dynamical diffraction gives rise to diffracted intensities that are difficult to interpret quantitatively. Another consequence of dynamical effects is that weak reflections such as those “forbidden” by symmetry commonly appear. These dynamical effects are commonly undesirable, particularly if we want to extract any information from the intensities of the spots, but in some cases may be welcome as they allow easy identification of the symmetry from the “forbidden” reflections.

By simple geometric considerations, it can be demonstrated that the d_{hkl} spacing of a given spot can be calculated by dividing a constant by the distance to the central spot in the diffraction pattern. This camera constant is the product of the wavelength of electrons by the so-called camera length, which, in diffraction, plays a role equivalent to magnification in the images. Nevertheless, the camera constant can be affected by a number of factors, including distortions, and it is far from its theoretical value; therefore, precision and accuracy are clearly worse than for X-ray diffraction, but can be approximated to 0.1% if distortion is corrected by the Capitani *et al.* (2006) method and some basic guidelines are respected (Mugnaioli *et al.* 2008). As a diffraction pattern is a representation of the reciprocal space, in a similar way to X-ray diffraction, shorter distances represent longer d spacings.

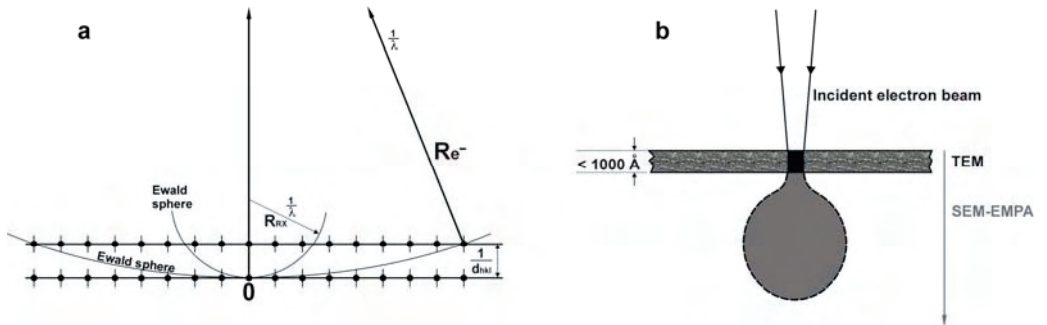


FIGURE 3. a) Schematic diagram of the Ewald sphere for electrons and X-rays. The radius ($R=1/\lambda$) is far greater for electrons, and therefore more reciprocal-lattice points (which represent the crystallographic planes) are intersected for a given orientation. Consequently, the pattern is essentially tangent over a large region of the reciprocal space and many diffraction spots can be recorded without any sample motion. The effect is accentuated by the extremely thin samples, which produce extended reciprocal lattice spikes (vertical lines superposed on the spots). λ = wavelength, d_{hkl} = spacing between crystallographic planes. Modified from Buseck (1992). b) Comparison of the electron-excited areas between thick (grey area) and thin (black area) samples.

Lattice images

A surplus of the electron diffraction facility in the microscope is the possibility of acting on the images, selecting the rays used to construct the images using appropriate apertures. If we use only one diffracted or transmitted ray, we obtain amplitude contrast, producing respectively dark or bright field images. They do not have lattice resolution and consequently this technique is termed conventional TEM.

By contrast, if we select a combination of rays with d_{hkl} spacing higher than the nominal resolution of the microscope, we allow the rays to interfere each other, thereby producing phase contrast images, which contain information about the crystallographic structure of the sample. They are usually termed high-resolution images (HRTEM), but in most cases give information only about lattice periodicity—including local defects—due to which their correct name would be lattice (fringe) images in contrast to structure images. A structure image would be directly interpretable without previous knowledge of the crystal structure; only in this case an atom produce black spots and voids white ones.

One of the basic conditions to obtain structure images is that the microscope focus be adjusted to the value in which the contrast transfer function has its greatest trough, that is, the so-called Scherzer focus, which is specific to each particular TEM. The contrast transfer function describes the imperfections in the lens system that result in modifications to the amplitudes and phases of the electron beams, producing distortions of the images due to the prevention of proper interference of the waves.

Electron crystallography

X-ray diffraction produces structural information in which the crystallographic characteristic of all the cells of the diffracting crystal are mediated; in this way, we obtain an average structure in which individual defects are ignored and potentially avoided. By contrast, TEM concentrates its power on the proper identification of such defects. This has, in part, been the reason for the great success of TEM in geology in recent years. Nevertheless, electron microscopists are exploring the possibilities of HRTEM and electron diffraction to determine the crystallographic structure of fine-grained and defective materials.

A high-resolution image is a more-or-less distorted representation of the atomic distribution in the sample. Two basic methods have been employed to properly interpret such information. The first one is image simulation, which calculates expected images from the structure of the sample and the technical conditions of TEM. In this manner, the experimental images can be compared with a limited number of hypothetical structures. The second method is the direct interpretation of the images. Electron crystallography software is able to produce Fourier transforms of the experimental images, producing something like virtual electron diffraction. A second Fourier transform would give the original image again, but with all the cells and symmetric parts of the each cell mediated; finally, the effects of the contrast transfer function can be subtracted, thereby mathematically producing a virtual structural image.

The other way in which electron crystallography works is to use the intensities of electron diffraction in a similar way to those of X-ray diffraction. Here also two different methods have been employed. One method tries to minimize dynamical effects by obtaining the electron diffraction from very thin areas, hence it uses the same software as X-ray diffraction. The other method assumes the presence of dynamical effects and uses

a completely different system of structural analysis based on the dynamical diffraction theory.

Analytical electron microscopy (AEM)

The intensity of a given emission line is proportional to the concentration of the corresponding element. In thick samples, the beam penetrates to considerable depth (Fig. 3b). The resulting X rays emitted are subject to absorption and fluorescent effects. Nevertheless, in the thin electron-transparent films generally used in TEM, the paths of emitted X-rays are so short that absorption and fluorescence can be neglected. This is the so-called Cliff-Lorimer (Cliff and Lorimer, 1975) approximation. The ratio of atomic concentrations of two elements (c_a/c_b) is directly proportional to the ratio of the intensities of the emission lines of those elements (I_a/I_b). Only a proportionality factor K_{ab} is necessary to calculate the relative amount of the elements from the measured intensities. Therefore, it is a relative method in which the concentration ratios of elements can be known, but not their absolute quantities. This is a basic limitation of the technique, but it is not particularly limiting in mineralogy as mineral compositions are usually normalized to their formulae. To present an analysis in the form of oxides in the traditional fashion is artificial and may be misleading. It is the concentration ratios (formulae) that should normally be presented as the basic AEM data.

The software of EDX equipment contains theoretical K factors, calculated from first principles (Goldstein et al., 1986) to be used in the so-called *standardless analyses*. Nevertheless, the K factors need to be experimentally determined for a standard of known composition, as they are valid only for values obtained under specific conditions for a specific instrument. In fact, should the counter window or crystal be replaced, large changes in K-values are possible. Therefore, *standardless analyses* produce only approximate results very far from being considered quantitative.

Electron energy-loss spectroscopy (EELS)

The energy lost by beam electrons during inelastic interactions is converted into secondary signals as X-rays, cathodoluminescence, and Auger electrons. In addition to these signals, the changes in energies of the beam electrons also provide information about both the types of atoms in the specimen and about their chemical states (bonding,

valence, coordination). Electron energy-loss spectroscopy, or EELS for short, is the measurement of the energy distribution of electrons that have passed through a specimen.

EELS reflects a primary event of energy change, in contrast with EDX, which reflects a secondary event, the energy of radiation released upon relaxation during the return of the atom to its ground state. Since most electrons that cause ionization can be collected by the EELS spectrometer, the method has high detection efficiency. In comparison to EDX, EELS is better suited for light elements, with the possibility of measuring up to Li. In general, quantification of EELS spectra is more difficult and the results less accurate than for EDX because of the broad shapes of the EELS edges and the high background.

Elemental and chemical analysis is probably the major application of EELS for mineralogy, but the spectra contain far more information. Valence states and local environments of atomic species can be determined from EELS spectra by using EXELFS (extended energy-loss fine structure) and ELNES (energy-loss near-edge fine structure). Small changes in the edge energy are caused by differences in valence state. These chemical shifts can be used to determine the valence states of elements in a specimen; this technique has been successfully applied to a variety of minerals. It is difficult to obtain such information at such a fine spatial resolution by any other technique. Nevertheless, while it is easy to see changes in oxidation states, one limitation is that it is difficult to quantify their fractions.

Applications

The scales for the observation of geological phenomena range from 10^6 m for plate tectonics to 10^{-10} m for mineral lattices. Many characteristics may be recognized in such a wide range of dimensions with similar meaning (e.g. folds). The various sub-techniques included in TEM, presented above, allow the observation and study of a plethora of phenomena—among them the following can be mentioned as examples.

- Electron diffraction

Identification, orientation, and cell parameters of minerals.

- Images (low or high resolution)

Mosaic crystal, twins, dislocations, strain, polytypism, polysomatism, phase transformation, antiphase domains, nanotextures, nanocrystals, exsolution, non-stoichiometry.

- Analytical electron microscopy

Quick mineral identification, high-spatial resolution quantitative analysis.

The frequent use of TEM in the geological sciences has revealed that many of these phenomena are more the rule than the exception. Mellini (1985) proposed the concept of microstructure to define “defects of various types and origins inside a monomineral grain (definable as real structure in a strict sense) or the diverse associations of several minerals in a polyphasic grain, homogeneous on a macroscopic scale” The first part of the definition has been a well-known concept in crystallography for decades, even considered in some definitions of crystals (Navrotsky, 1994), while the second part begins to point to a redefinition of the concept of mineral itself. The occurrence of a given microstructure mainly depends on the nucleation conditions and/or on the post-crystallization sub-solidus evolution. They may be important indicators of the thermobaric evolution of minerals and rocks.

TABLE 1 refers to some representative examples, ordered according to the type of phenomenon studied. In addition, some significant cases are presented below.

PHENOMENON	REFERENCE
POLYMORPHISM	
Reconstructive transformations	
-Three different polymorphs of wollastonite in the Allende meteorite	Brenker and Krot (2004)
-Biogenic nanocrystalline sphalerite and wurtzite growing on degraded wood	Moreau <i>et al.</i> (2004)
-Berthierine and chlorite: stability relationships; are they true polymorphs?	Abad-Ortega and Nieto (1995)
-Microstructures of polygonal serpentines	Baronnet and Devouard (2005)
-Martensitic transition due to decompression in α -PbO ₂ -type TiO ₂ in ultra-high-pressure metamorphic rock	Shen <i>et al.</i> (2005)
Displacive transformations	
-Antiphase domains in pigeonite	Moore <i>et al.</i> (2001)
-Twin walls in anorthoclase enriched in alkali and depleted in Ca and Al	Camara <i>et al.</i> (2000)
Order-disorder transformations	
-Antiphase domains in omphacites	Brenker <i>et al.</i> (2003)
-Antiphase domains in scapolite solid solutions	Seto <i>et al.</i> (2004)
-Niocalite. False disordered distribution of Nb and Ca, due to polysynthetically twinned domains	Mellini (1982)
Fe/Cu ordered superstructure of bornite	Ding <i>et al.</i> (2005)
Fe/Mg ordering in low-calcium actinolite	Driscall <i>et al.</i> (2005)
POLYTYPISM	
-Micas	Amouric <i>et al.</i> (1981)
-Kaolinite-dickite	Kogure and Inoue (2005)
-Chlorites	Spinkler <i>et al.</i> (1984)
-Lizardite-chlorite transformation and high-pressure lizardite polytype	Dodony and Buseck (2004)
-Disorder across the interlayer region in sodium mica wonesite	Kogure <i>et al.</i> (2005)
-Parallel intergrowths in cronstedtite	Durovic <i>et al.</i> (2004)

POLYSOMATISM	
-Structural modulation of antigorites	Viti and Mellini (1996)
-Pyribole evolution during tremolite synthesis (non-amphibole chain multiplicity faults)	Bozhilov <i>et al.</i> (2004)
-Polysomatic faults and structural imaging in antigorite	Capitani and Mellini (2005)
-Chain multiplicity faults in deformed and recovered omphacite	Muller <i>et al.</i> (2004)
Interstratified minerals	
-Interstratification of 2:1 layer-silicates studied by alkylammonium ion treatment	Vali and Köster (1986)
-Illite-smectite mixed-layering	Olives <i>et al.</i> (2000)
-Interstratification of Na/K interlayers in aspidolite, the Na analogue of phlogopite	Kogure <i>et al.</i> (2004)
STRUCTURAL DEFECTS	
-Deformation microstructures in eclogites	Muller and Franz (2004)
-Dislocations and plasticity of experimentally deformed coesite	Idrissi <i>et al.</i> (2008)
-Deformation and recrystallisation mechanisms in naturally deformed omphacites	Buatier <i>et al.</i> (2004)
Alteration and deformation microstructures of biotite	Sanchez-Navas and Galindo-Zaldivar (1993)
TRANSFORMATIONS WITH CHEMICAL CHANGE	
Exsolution	
-Augite and pigeonite lamellae in meteorites. Thermal histories of basaltic eucrites from Vesta	Schwartz and McCallum (2005)
-Topotaxially concordant amphibole exsolution lamellae in garnet from ultrahigh-pressure rocks	Song <i>et al.</i> (2005)
-Exsolution microstructures in a complex amphibole assemblage from metabasalts	Ruiz Cruz <i>et al.</i> (2007)
Non-stoichiometry	
- Massive and lamellae amphiboles within clinopyroxenes of Coronas in anorthosites	Mellini <i>et al.</i> (1983)
-Invisible gold in As-rich overgrowths on pyrite	Palenik <i>et al.</i> (2004)

False stoichiometry	
-Native copper inclusions in biotites of porphyry copper deposits	Ilton and Veblen (1988)
-Iron in rutile	Banfield and Veblen (1991)
ELECTRON CRYSTALLOGRAPHY	
-Basics	Zou (1995)
-Crystallographic Image-Processing of high-resolution images of bannisterite	Ferrow and Hovmoller (1993)
-Crystal structure of parsettensite determined using electron diffraction patterns	Eggleton and Guggenheim (1994)
-Crystal structure of “iscorite” described anew from Fourier-filtering analyses of HRTEM images in combination with SAED data	Van Aken <i>et al.</i> (2005)
-Electron-Diffraction of Textures	Zvyagin (1994)
NANOCRYSTALS	
-Syntheses of magnetite nanocrystals: morphology, crystal size, and shape ratio. Implications for formation conditions	Faivre <i>et al.</i> (2005)
-Exclusively inorganic formation of magnetite in Martian meteorite	Golden <i>et al.</i> (2004)
-Vaterite precipitation in the microenvironment around bacterial cells	Rodriguez-Navarro <i>et al.</i> (2007)
-Irreversible colloidal behavior of Ca(OH) ₂ in lime mortars and plasters	Rodriguez-Navarro <i>et al.</i> (2005)
-Spherical aggregates of kaolinite crystallized via in-situ transformation of gels	Huertas <i>et al.</i> (2004)
-Bacterially-mediated authigenesis of clays phosphate stromatolites	Sánchez Navas <i>et al.</i> (1998)

PETROGRAPHY OF FINE-GRAINED MATERIALS	
-Smectite-illite diagenetic transformation	Ahn and Peacor (1986)
-Prograde and retrograde diagenetic and metamorphic evolution in metapelitic rocks	Abad et al (2003)
-Nanometer-sized meteorite impact-derived glass	Bauluz <i>et al.</i> (2004a)
-Mineral composition and genetic relationships in impactite	Ding and Veblen (2004)
-Direct transformation of andalusite to kaolinite in strongly deformed areas	Jimenez-Millan <i>et al.</i> (2007)
-Submicroscopic intergrowths of K biotite, Na biotite, and intermediate Na-K biotite	Ruiz Cruz (2004)
-Nanometric intergrowths of graphite within ultramafic phlogopite	Ferraris <i>et al.</i> (2004)
-Mineralogical characterisation of archaeological pottery	Giorgetti <i>et al.</i> (2004)
-Environmentally important, poorly crystalline Fe/Mn hydrous oxides	Hochella <i>et al.</i> (2005)
-Mineral transformations in fired carbonated clays	Bauluz <i>et al.</i> (2004b)
-Evolution of textures and mineral assemblages from sediment to metamorphic rock in open hydrothermal systems	Giorgetti <i>et al.</i> (2003)

The polymorphs of TiO₂

Seven known polymorphs of TiO₂ exist. Rutile, anatase, and brookite had been previously found in nature. Nevertheless, in anatase Bandfield *et al.* (1991) found lamellae of a second mineral, ranging in size from a few nm to hundreds of a nm across. Both minerals showed a well-defined orientation relationship but the interplanar spacings of lattice parallel to the interphase were not exactly equal. They interpreted high-resolution electron micrographs to determine the positions of columns of Ti cations within the unit cell. The model structure was tested by comparing computer-generated images with experimental micrographs and refined using a distance-least-squares program to adjust interatomic distances to those previously known in anatase and rutile. The unnamed mineral had been reported previously as the synthetic polymorph TiO₂ (B). In this way, they were able to model the structure of anatase, TiO₂ (B), and their

boundaries. Heating experiments carried out with the electron microscope showed that TiO₂ (B) was converted to anatase at a furnace temperature of ~700 °C (~100 °C below the anatase-rutile transformation).

The most common form of TiO₂ in nature is rutile, which is an important accessory mineral in metamorphic rocks, particularly high-pressure ones. Wu *et al.* (2005) described a natural high-pressure phase of titanium oxide with α -PbO₂-structure. It occurred as (<20 Å) lamellae between multiple twinned rutile crystals in coesite-bearing eclogite at Shima in the Dabie Mountains, China. These lamellae presented an orthorhombic lattice, corresponding to α -PbO₂-type TiO₂ with space group Pbcn. The α -PbO₂-type TiO₂ could be an extremely useful index mineral for ultrahigh pressure. Diamond in the mineral assemblage of Dabie Mountains indicates the metamorphic conditions to be greater than a pressure of 4 GPa (Xu *et al.* 1992). Based on the TiO₂ phase boundary reported by Withers *et al.* (2003), the α -PbO₂-type nanophase of TiO₂ in rutile records a minimum pressure of 7 GPa (depth of more than 200 kilometres).

Antiphase domains

High pigeonite has symmetrically equivalent Si-O tetrahedral chains, but in low pigeonite there are two symmetrically distinct chains, each with a different degree and sense of rotation. With a decrease in temperature, the polymorphic change produces the two types of chains, which lose their equivalence (Putnis, 1993); as the change does not match up in the different areas of the mineral, there is the possibility of the formation of an interface across which the sequence of chains is incorrect. Such domains are called antiphase domains.

Since they involve only translational differences, antiphase domains cannot be seen by optical microscopy. However, the loss of symmetry between the two types of chains produces the change from a C-centred to a primitive unit cell (Putnis, 1993). Dark-field electron micrographs using reflections of the type $h+k = \text{odd}$, which are present in P lattice but absent in C lattice, allow the antiphase domains to be identified and their boundaries to be recognised.

In omphacites, and in many other minerals (e.g. plagioclases), two cations, or more, share a site. With a decrease in temperature, each cation “chooses” its own exclusive site. Such a differentiation of crystallographic sites may even produce a change in the

space group. The low-temperature polymorph is a sub-group of symmetry of the high-temperature one. The loss in translational symmetry in order-disorder transformations can also produce antiphase domains (Brenker *et al.* 2003).

The mean antiphase domain size and form depend on peak temperature, duration of peak metamorphism, cooling rate, and composition. They therefore provide very useful information about the geological history of the minerals.

Retrograde intergrown phyllosilicate grains

Phyllosilicate grains, showing optical characteristics identical to biotite, are frequent. They differ in mineral nature, composition, and origin, and may be grains corresponding to a single mineral or a combination of two or more mineral species. One of the most significant cases was described in the Alps by Chatterjee (1966), who gives it the name “oxidized chlorites” due to its basically chloritic composition. Grains with the same optical and chemical characteristic are rock-forming minerals in the graphite schists of the Nevado-Filabride Complex in the Internal Zones of the Betic Cordillera. Based on Chatterjee’s description in the Alps, the Nevado-Filabride grains were also considered as oxidized chlorites. Nevertheless, Mellini *et al.* (1991) recognised that most of the area was dominated by 14 Å lattice fringes, with chlorite composition, but smectite was also present as individual 10Å layers interlayered in the chlorite or as packets a few layers thick. In other areas, a poorly crystalline 16Å phyllosilicate with chlorite composition, interpreted as hydrated chlorite, was recognised in addition to semi-amorphous material showing hematite spacings and composition.

All these supergenic-origin materials were interpreted as the result of fluid-mediated processes in relation to the uplift of the Nevado-Filabride rocks, due to erosion and/or post-metamorphic extension. A similar process was later described in the overlying Malaguide Complex by Nieto *et al.* (1994). These two cases were some of the first retrograde alteration processes, which, together with numerous other examples, were employed some years later (Nieto *et al.* 2005) to define *retrograde diagenesis*.

Serpentine minerals

The serpentine tetrahedral and octahedral layers present partially different dimensions along the **a** and **b** directions. The various serpentine minerals display

different mechanisms that provide solutions to their fitting. For example, a rolled microstructure producing cylinders is a characteristic in TEM for recognising chrysotile. In contrast, the antigorite structure results from a structural modulation of the serpentine layers along the **a** direction. The shorter tetrahedral layers change their polarity every given number of sub-cells, passing from upper to lower position in relation to the longer octahedral layers (Capitani and Mellini, 2004). A selected area electron diffraction (SAED) pattern consists of the main diffraction spots from the sub-cell, which are surrounded by satellite diffraction spots from the modulated structure of antigorite. The *m*-values, representing the number of tetrahedra in one modulation, range from 13 to 50 and can be determined from the respective spacings of the sub-cell and the modulated structure. Antigorite microstructures vary from highly ordered to lower periodic structures in the *c* direction (Auzende *et al.* 2006). TEM is a convenient tool for investigating and characterising antigorite variability at such a scale. Serpentine microstructures can potentially preserve information on metamorphic conditions.

The deformation processes of serpentinites during subduction are complex. According to microstructural evidence, shearing is accommodated by brittle and/or ductile deformation mechanisms. With increasing metamorphic grade, the brittle behaviour gives way to pressure solution, which persists up to eclogite-facies conditions. Once the partial dehydration reaction is reached, antigorite may recrystallise, mainly by a pressure-solution mechanism. The required fluids would derive from the progressive dehydration of antigorite (Auzende *et al.* 2006). Pressure solution is an effective mechanism to accommodate deformation; according to these authors, serpentinites could localize the deformation within a subduction/exhumation channel, thus making it possible to preserve eclogites from depths of about 100 km below the Earth's surface.

Ammonium micas

The common interlayer cations in low-grade metapelite micas are K and Na. In addition, since the late 1950s, ammonium has been recognised as an important interlayer constituent in white micas associated with organic matter. This third important interlayer component had not been thoroughly studied due, in part, to the intrinsic difficulty of analyzing NH_4 by *in-situ* methods and, in part, to the typically defective character and

small grain size of minerals in very low-grade metamorphic rocks, since most natural tobelites have been described in subgreenschist-facies rocks.

Nieto (2002) was the first to describe, using TEM, the textural characteristics of NH_4 micas in very low-grade metapelites with associated coal seams (from the *Bacia Carbonífera do Douro-Beira*, N Portugal), and he established their chemical and genetic relationships with coexisting K micas. NH_4 and K micas and berthierine form small subparallel packets of a few layers separated by low-angle boundaries, exhibiting all the characteristics commonly described for subgreenschist-facies, which includes a lack of textural and chemical equilibrium. In the Douro-Beira samples, the simultaneous presence of two groups of compositions of micas, one K-rich and the other K-poor, was demonstrated by XRD, lattice fringe images, electron diffraction, and analytical electron microscopy data (Fig. 4). The textural relationship between the two micas was the usual one between paragenetic phyllosilicates in very low-grade shales, like the one described for the muscovite/paragonite system by Shau *et al.* (1991). NH_4 - and K-dominated micas were segregated into well-separated packets with scarce intergrowth and almost no mixed-layers. Hence, they showed a solvus relationship. The compositional gap is narrow (Fig. 4), possibly near closure.

The presence of N in the micas was also confirmed by electron energy loss spectroscopy (EELS) of powdered portions dispersed on holey-carbon grids (Livi *et al.* 2006). The method involves a simultaneous acquisition of EELS spectra over the energy-loss range 275-475 eV and the acquisition of energy dispersive X-ray spectra (EDS). The EELS spectra contain the core-loss edges for K L_{2,3} (296.3 eV) and N K (400.9 eV). Thus, the N/K ratio can be calculated. Analysis of ammonium in white micas from the Central Alps, Switzerland, indicated that concentrations of N down to 0.01 atoms per formula unit could be detected.

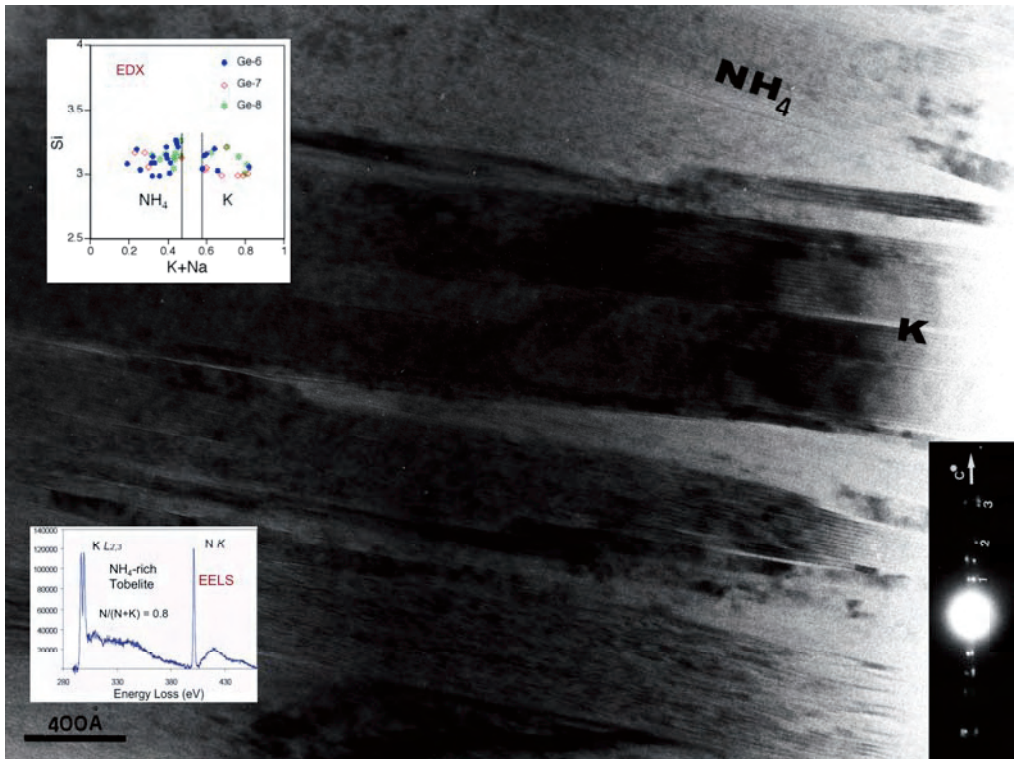


FIGURE 4. Lattice-fringe image showing textural relationships between packets of muscovite (K) and tobelite (NH_4) in an organic-rich shale. Insets: Chemical contents of three samples determined by EDX, showing the gap between the two kinds of micas; K/N ratio of a tobelite crystal determined by EELS; electron diffraction pattern (bottom right) in which the existence of two slightly different (00l) spacings is evident in the third (3) order. The intermediate spot between second (2) and first (1) order corresponds to a minor local muscovite/tobelite mixed-layer (not visible in the image). From Nieto (2002) and Abad *et al.* (2007).

Genesis of Mn oxides from marine sediments

Mn oxy-hydroxides form as a result of diagenetic, hydrogenous, or hydrothermal processes along mid-ocean ridges or on the sea floor, using reduced dissolved Mn^{2+} provided by springs. These oxides, which have a +3 or +4 valence state, are largely controlled by redox and pH conditions. Precipitation of Mn oxy-hydroxide in natural environments could result from microbial processes, which accelerate the rate of Mn^{2+} oxidation. Buatier *et al.* (2004) studied Mn deposits and partially altered sediments from the flank of the Juan de Fuca Ridge. At SEM scale, samples exhibited abundant

encrustations of detrital grains and fossils by Mn oxy-hydroxides, suggesting that the oxides formed from the interaction of fluids with sediments.

Well-crystallised Mn-oxide phases were todorokite and birnessite, based on XRD, TEM, and SAED analyses of Mn crusts. TEM and SAED allowed the identification of poorly crystallized and amorphous phases with small crystal size that could correspond to poorly crystallized birnessite and amorphous Mn-rich nanocrystallites, also containing Si and Fe.

To determine the valence of Mn in the different types of particles, the MnL_3 to MnL_2 area ratio was measured and compared with that of three standard samples containing Mn^{2+} , Mn^{3+} , and Mn^{4+} respectively. The valence of Mn was then calculated from the calibration curve. The chemical shift of the MnL_3 edge was also measured for the different types of particles and compared to standard samples. The shape of the oxygen K-edge spectra of the samples was also observed and compared with that of standard compounds. EELS analyses gave an average oxidation state for Mn of about 3.7 for birnessite and a lower average valence state for veil-like particles and aggregates of small veil-forming cellular structures of filament.

Buatier *et al.* (2004) concluded that todorokite was the final product requiring a several-step mechanism for formation. This implies that reactants included intermediate lower-valence state and poorly crystallized minerals, with progressive increases in the size and crystallinity of Mn oxide and a progressive oxidation of Mn.

References

- Abad, I., Livi, K., Nieto, F., Árkai, P. and Judik, K. (2007). Analysis of ammonium in micas by Electron Energy-Loss Spectroscopy, in "Diagenesis and Low-Temperature Metamorphism. Theory, Methods and Regional Aspects", F. Nieto and J. Jiménez-Millán, eds. Seminarios SEM 3, 99.
- Abad, I., Nieto, F., Peacor, D.R. and Velilla, N. (2003). Clay Miner., 38, 1-23.
- Abad-Ortega, M.A. and Nieto, F. (1995). Contrib. Mineral. Petrol., 120, 327-336.
- Ahn, J.H. and Peacor, D.R. (1986). Clays Clay Miner., 34, 165-179.
- Amouric, M., Mercurio, G. and Baronnet, A. (1981). Bull. Miner., 104, 298-313.
- Auzende, A.L., Guillot, S., Devouard, B. and Baronnet, A. (2006). Eur. J. Mineral., 18, 21-33.
- Banfield, J.F., Veblen, D.R. and Smith, D.J. (1991). Am. Mineral., 76, 343-353.
- Banfield, J.F. and Veblen, D.R. (1991). Am. Mineral., 76, 113-127.
- Baronnet, A. and Devouard, B. (2005). Can. Mineral., 43, 513-542.

- Bauluz, B., Mayayo, M.J., Yuste, A., Fernandez-Nieto, C. and Gonzalez Lopez, J.M. (2004a). *Clay Miner.*, 39, 333-344.
- Bauluz, B., Peacor, D.R. and Hollis, C.J. (2004b). *Earth Planet. Sci. Lett.*, 219, 209-219.
- Bozhilov, K.N., Jenkins, D.M. and Veblen, D.R. (2004). *Am. Mineral.*, 89, 74-84.
- Brenker, F.E. and Krot, A.N. (2004). *Am. Mineral.*, 89, 1280-1289.
- Brenker, F.E., Muller, W.F. and Brey, G.P. (2003). *Am. Mineral.*, 88, 1300-1311.
- Buatier, M.D., Guillaume, D., Wheat, C.G., Herve, L. and Adatte, T. (2004). *Am. Mineral.*, 89, 1807-1815.
- Buseck, P.R. (1992). Principles of transmission electron microscopy, in "Minerals and reactions at the atomic scale: transmission electron microscopy", P.R. Buseck, ed. *Min. Soc. Amer. Reviews in Mineralogy* 27, 1-35. Washington, D.C.
- Camara, F., Doukhan, J.C., Domeneghetti, M.C. and Zema, M. (2000). *Eur. J. Mineral.*, 12, 735-748.
- Capitani, G. and Mellini, M. (2004). *Am. Mineral.*, 89, 147-158.
- Capitani, G. and Mellini, M. (2005). *Am. Mineral.*, 90, 991-999.
- Capitani, G.C., Oleynikov, P., Hovmoller, S. and Mellini, M. (2006). *Ultramicroscopy*, 106, 66-74.
- Chatterjee, N.D. (1966). *Contrib. Miner. Petrol.*, 12, 325-339.
- Cliff, G. and Lorimer, G.W. (1975). *Journal of Microscopy*, 103, 203-207.
- Ding, Y. and Veblen, D.R. (2004). *Am. Mineral.*, 89, 961-968.
- Ding, Y., Veblen, D.R. and Prewitt, C.T. (2005). *Am. Mineral.*, 90, 1265-1269.
- Dodony, I. and Buseck, P.R. (2004). *Am. Mineral.*, 89, 1631-1639.
- Driscoll, J., Jenkins, D.M., Dyar, M.D. and Bozhilov, K.N. (2005). *Am. Mineral.*, 90, 900-911.
- Durovic, S., Hybler, J. and Kogure, T. (2004). *Clays Clay Miner.*, 52, 613-621.
- Eggleton, R.A. and Guggenheim, S. (1994). *Am. Mineral.*, 79, 426-437.
- Faivre, D., Menguy, N., Guyot, F., Lopez, O. and Zuddas, P. (2005). *Am. Mineral.*, 90, 1793-1800.
- Ferraris, C., Grobety, B., Fruh-Green, G.L. and Wessicken, R. (2004). *Eur. J. Mineral.*, 16, 899-908.
- Ferrow, E.A. and Hovmoller, S. (1993). *Eur. J. Mineral.*, 5, 181-188.
- Giorgetti, G., Gliozzo, E. and Memmi, I. (2004). *Eur. J. Mineral.*, 16, 493-503.
- Giorgetti, G., Mata, M.P. and Peacor, D.R. (2003). *Clay Miner.*, 38, 113-126.
- Golden, D.C., Ming, D.W., Morris, R.V., Brearley, A., Lauer, H.V., Treiman, A.H., Zolensky, M.E., Schwandt, C.S., Lofgren, G.E. and McKay, G.A. (2004). *Am. Mineral.*, 89, 681-695.
- Hochella, M.F., Kasama, T., Putnis, A., Putnis, C.V. and Moore, J.N. (2005). *Am. Mineral.*, 90, 718-724.
- Huertas, F.J., Fiore, S. and Linares, J. (2004). *Clay Miner.*, 39, 423-431.
- Idrissi, H., Cordier, P., Jacob, D. and Walte, N. (2008). *Eur. J. Mineral.*, in press.
- Ilton, E.S. and Veblen, D.R. (1988). *Nature*, 334, 516-518.
- Jimenez-Millan, J., Velilla, N. and Vazquez, M. (2007). *Clay Miner.*, 42, 273-286.
- Kogure, T., Banno, Y. and Miyawaki, R. (2004). *Eur. J. Mineral.*, 16, 891-897.
- Kogure, T. and Inoue, A. (2005). *Eur. J. Mineral.*, 17, 465-473.
- Kogure, T., Miyawaki, R. and Banno, Y. (2005). *Am. Mineral.*, 90, 725-731.

- Livi, K., Abad, I., Nieto, F. and Veblen, D. (2006). Geophysical Research Abstracts, 8, 09739.
- Mellini, M. (1982). *Tschemaks Min. Petr. Mitt.*, 30, 249-266.
- Mellini, M. (1985). *Rend. Soc. Ital. Min. Petrol.*, 40, 229-240.
- Mellini, M., Nieto, F., Alvarez, F. and Gómez-Pugnaire, M.T. (1991). *Eur. J. Mineral.*, 3, 27-38.
- Mellini, M., Oberti, R. and Rossi, G. (1983). *Periódico di Mineralogia. Roma.*, Anno 52, 538-615.
- Moore, K.T., Veblen, D.R. and Howe, J.M. (2001). *Am. Mineral.*, 86, 1314-1318.
- Moreau, J.W., Webb, R.I. and Banfield, J.F. (2004). *Am. Mineral.*, 89, 950-960.
- Mugnaioli, E., Capitani, G., Nieto, F. and Mellini, M. (2008). *Am. Mineral.*, in press.
- Muller, W.F., Brenker, F.E., Barnert, E.B. and Franz, G. (2004). *Eur. J. Mineral.*, 16, 37-48.
- Muller, W.F. and Franz, G. (2004). *Eur. J. Mineral.*, 16, 939-944.
- Navrotsky, A. (1994) *Physics and Chemistry of Earth Materials*. Cambridge University Press, 417 pp.
- Nieto, F. (2002). *Am. Mineral.*, 87, 205-216.
- Nieto, F., Mata, M.P., Bauluz, B., Giorgetti, G., Árkai, P. and Peacor, D.R. (2005). *Clay Miner.*, 40, 93-104.
- Nieto, F., Velilla, N., Peacor, D.R. and Ortega-Huertas, M. (1994). *Contrib. Mineral. Petrol.*, 115, 243-252.
- Olives, J., Amouric, M. and Perbost, R. (2000). *Clays Clay Miner.*, 48, 282-289.
- Palenik, C.S., Utsunomiya, S., Reich, M., Kesler, S.E., Wang, L.M. and Ewing, R.C. (2004). *Am. Mineral.*, 89, 1359-1366.
- Putnis, A. (1993). *Introduction to mineral sciences*. Cambridge University Press. Cambridge. 457 pp.
- Rodriguez-Navarro, C., Jimenez-Lopez, C., Rodriguez-Navarro, A., Gonzalez-Munoz, M.T. and Rodriguez-Gallego, M. (2007). *Geochim. Cosmochim. Acta*, 71, 1197-1213.
- Rodriguez-Navarro, C., Ruiz-Agudo, E., Ortega-Huertas, M. and Hansen, E. (2005). *Langmuir*, 21, 10948-10957.
- Ruiz Cruz, M.D. (2004). *Clays Clay Miner.*, 52, 603-612.
- Ruiz Cruz, M.D., Puga, E. and De Federico, A. (2007). *Eur. J. Mineral.*, 19, 547-556.
- Sánchez Navas, A., Martín Algarra, A. and Nieto, F. (1998). *Sedimentology*, 45, 519-533.
- Sanchez-Navas, A. and Galindo-Zaldivar, J. (1993). *Eur J Mineral*, 5, 245-256.
- Schwartz, J.M. and McCallum, I.S. (2005). *Am. Mineral.*, 90, 1871-1886.
- Seto, Y., Shimobayashi, N., Miyake, A. and Kitamura, M. (2004). *Am. Mineral.*, 89, 257-265.
- Shau, J.H., Feather, M.E., Essene, E.J. and Peacor, D.R. (1991). *Contrib. Mineral. Petrol.*, 106, 367-378.
- Shen, P.Y., Hwang, S.L., Chu, H.T., Yu, T.F., Pan, C.N. and Huang, W.L. (2005). *Eur. J. Mineral.*, 17, 543-552.
- Song, S.G., Zhang, L.F., Chen, J., Liou, J.G. and Niu, Y.L. (2005). *Am. Mineral.*, 90, 814-820.

- Spinkler, G.E., Self, P.G., Lijama, S. and Buseck, P.R. (1984). *Am. Mineral.*, 69, 252-263.
- Vali, H. and Köster, M. (1986). *Clay Min.*, 21, 827-859.
- Van Aken, P.A., Mische, G., Woodland, A.B. and Angel, R.J. (2005). *Eur. J. Mineral.*, 17, 723-731.
- Viti, C. and Mellini, M. (1996). *Eur. J. Mineral.*, 8, 423-434.
- Withers, A.C., Essene, E.J. and Zhang, Y.X. (2003). *Contrib. Mineral. Petrol.*, 145, 199-204.
- Wu, X.L., Meng, D.W. and Han, Y.J. (2005). *Am. Mineral.*, 90, 1458-1461.
- Xu, S.T., Okay, A.I., Ji, S.Y., Sengor, A.M.C., Wen, S., Liu, Y.C. and Jiang, L.L. (1992). *Science*, 256, 80-82.
- Zou, X. (1995). Thesis Univ. of Stockholm, 523 pp.
- Zvyagin, B.B. (1994). *Kristallografiya*, 39, 283-290.